Optical fiber sensor based on the short-range surface plasmon polariton mode

Xiaoyan Wang (王晓妍), Fang Liu (刘 仿)*, Ao Liu (刘 奥), Boyu Fan (樊博宇), Kaiyu Cui (崔开宇), Xue Feng (冯 雪), Wei Zhang (张 巍), and Yidong Huang (黄翊东)

State Key Laboratory of Integrated Optoelectronics, Department of Electronic Engineering, Tsinghua University, Beijing 100084, China

**Corresponding author: liu_fang@mail.tsinghua.edu.cn*

Received September 5, 2013; accepted November 28, 2013; posted online January 8, 2014

An optical fiber sensor for ultrathin layer sensing based on short-range surface plasmon polariton (SRSPP) is proposed, and the sensing characteristics are theoretically analyzed. Simulation results indicate that even for a detecting layer much thinner than the vacuum wavelength, a resolution as high as 3.7×10^{-6} RIU can be obtained. Moreover, an average thickness-detection sensitivity of 6.2 dB/nm is obtained, which enables the sensor to detect the thickness variation of the ultrathin layer up to tens of nanometers. The sensitive region of thickness could be adjusted by tuning the structure parameters.

OCIS codes: 060.2370, 250.5403, 280.1415.
doi: 10.3788/COL201412.010602.

Surface plasmon polariton (SPP) is a transverse magnetic surface electromagnetic wave that propagates along the interface of a metal and a dielectric medium[1]. Given the high sensitivity of the metal surface to changes in the refractive index of the substance[2], SPPs have shown great potential for chemical and biological sensing[2−6]. Optical fiber SPP sensors, which possess a myriad of advantages, (e.g., small size, high sensitivity, affordability, ease of manufacture, and potential for remote sensing), have attracted considerable attention. However, detection of bio- or chemical molecules requires the detecting layer to be about hundreds or tens of nanometers, which is thinner compared with the field size of a conventional SPP mode. The effective sensitivity of a conventional fiber optic SPP sensor would degrade dramatically upon application for ultrathin layer sensing[7].

The short-range SPP (SRSPP) mode is a SPP mode confined on a relatively thin metal film. Owing to the highly bounded field on the metal film[2], SRSPP has been adopted to improve the effective sensitivity of the sensor for ultrathin layer detection[7−10]. In this letter, a SRSPP mode is introduced into the optical fiber sensor, which aims to improve sensitivity for ultrathin layer detection. The operational principle and sensing characteristics of this sensor based on SRSPP modes are analyzed theoretically. Results showed that even for a detecting layer as thin as one-eighth of wavelength, the sensing resolution could reach as high as 3.7×10^{-6} RIU (refractive index units). Moreover, the sensor is also applicable for detecting thickness variations in the ultrathin layer. For a detection layer with thickness of tens of nanometers, the average thickness-detection sensitivity is 6.2 dB/nm, and the sensitive region of the detecting layer thickness can be extensively adjusted by varying the structural parameters.

Figure 1 shows the proposed optical fiber sensor based on SRSPP mode, which comprises three regions, namely, the input region I ($z < 0$), output region III ($z > L$), and the sensing region II ($0< z < L$). The operating wavelength λ_0 is 1550 nm. Meanwhile, region II is composed of a D-shaped single-mode fiber (SMF) (core radius $r_{\rm cor} = 5$ μm, residual radius $r_{\rm res} = 4$ μm), a SiO_2 dielectric layer (refractive index $n_{\rm d} = 1.444$[11] and thickness $h_{\rm d}$=0.5 μm), and an Au film (dielectric constant $\varepsilon_m = -132 + {\rm i}\times12.65$[11] and thickness $h_{\rm m}$ is initially fixed at 34 nm). Above the Au film is the detecting layer with varying refractive indices $n_{\rm det}$ and thicknesses $h_{\rm det}$. Different from the conventional SPP fiber sensor, a dielectric layer is introduced beneath the Au film, thereby applying the SRSPP mode in the sensor for ultrathin layer sensing.

The working principle of the proposed sensor is similar to that of the hybrid coupler based sensor on a chip[7,9,10]. If the refractive index of detecting layer is far from the crossing point of the blue and red curves (Fig. 2), the effective refractive indices of optical fiber guided and SRSPP modes would not be matched. In this case, the input energy would propagate across the entire fiber waveguide, and require a high output power from the fiber.

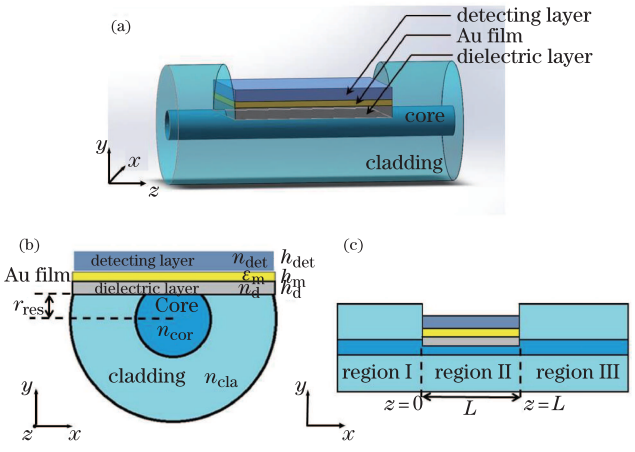

Fig. 1. Schematic structure of the proposed optical fiber sensor. (a) Three-dimensional view, (b) cross-sectional view in the $x-y$ plane, and (c) longitudinal view in the $y-z$ plane.

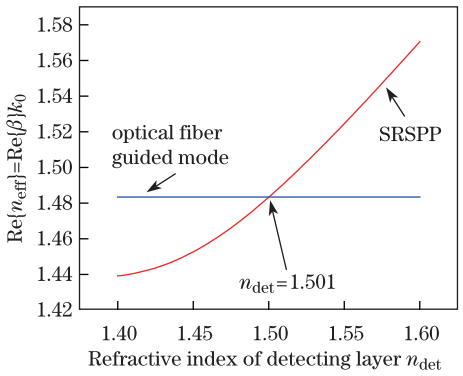

Fig. 2. Effective refractive index (Re{$n_{\rm eff}$}) of SRSPP (red) of an individual Au film part as a function of $n_{\rm det}$. The blue line corresponds to Re{$n_{\rm eff}$} of the optical fiber guided mode supported by an individual fiber part.

Assuming that the effective refractive indices of the optical fiber guided and SRSPP modes are equal, which corresponds to a crossing point, efficient coupling would occur between these modes, and the output power from the fiber would markedly reduce.

Based on the finite element method (FEM) using COMSOL software[12], the field distribution and propagation constants of the eigenmodes in all regions can be obtained. For the structural parameters, only one mode exists (HE_{11} mode) for a SMF in regions I and III, and two TM polarized eigenmodes (modes A and B) exist for the hybrid coupler structure in region II. Here, the HE_{11} mode with an electric component perpendicular to the metal film is referred to as "TM mode", which is assumed as the input and output modes in regions I and III. Figures 3(a)–(d) show the calculated field patterns of two eigenmodes in region II with a 500-nm-thick detecting layer when $n_{\rm det} = 1.501$. These eigenmodes with respective relative propagation constants $\beta_{\rm Ar}$, $\beta_{\rm Br}$ result from the opposite-phase and in-phase coupling between the individual SRSPP and optical fiber guided wave modes. The widths of dielectric layer, Au film, and the detecting layer are set at 10 μm to reduce computational complexity. Figures 3(e)–(h) show the real and imaginary parts of the primary electric field component $E_{\rm y}$ of these eigenmodes with different values of $n_{\rm det}$ along the symmetric axis of the fiber cross-section (the dotted line in Fig. 3). The black solid profile shows that the concentration of the mode fields surrounding the Au film and fiber core are almost equal when $n_{\rm det} = 1.501$ because the effective refractive indices Re{$n_{\rm eff}$} of individual SRSPP and fiber guided modes match well (Fig. 2). For $n_{\rm det} = 1.481$ and $n_{\rm det} = 1.400$, Re{$n_{\rm eff}$} of individual SRSPP deviates from the crossing point, which leads to unbalanced field concentrations surrounding the Au film and the fiber core (red dashed and blue dotted curves in Figs. 3(c)–(f)).

From the eigenmode expansion method (EEM), the input "TM mode" of SMF in region I can be expanded in terms of the superposition of two eigenmodes in region II at $z = 0$. After propagation of length L, the two eigenmodes in region II will couple to the output "TM mode" in region III at $z = L$. From Eqs. (1) and (2) of Ref. [9], the output power $P_{\rm out}$ of sensing region II can be expressed as a function of the length L (Fig. 4). When the thickness of the detecting layer is fixed at 500 nm with $n_{\rm det} = 1.501$, the output power declines rapidly along L with strong ripple. This oscillation indicates that the coupled energy exchanges completely between SRSPP and fiber guided modes. Coupled-mode theory states that the energy transfer results from various relative propagation constants of the two eigenmodes, thereby calculating the coupling length $L_{\rm c}$ as $z = L_{\rm c} = \pi/(\beta_{\rm Ar} - \beta_{\rm Br})$[13]. The peaks of each oscillation show linear attenuation, which result from the energy that diminishes constantly because of the high SRSPP mode loss. When the refractive index of the detecting layer deviates from $n_{\rm det} = 1.501$, $P_{\rm out}$ has a much weaker ripple and a smaller slope (red and blue lines in Fig. 4, respectively) because of the lower coupled energy to the high loss SRSPP mode from the fiber guided mode.

Furthermore, the sensing characteristics can be determined from the $P_{\rm out} - L$ curve with different refractive indices of the detecting layer, $n_{\rm det}$. Figure 5 plots $P_{\rm out}$ against $n_{\rm det}$, with the sensing length fixed at $L = 5 \times L_{\rm c} = 1127$ μm (blue solid line). $n_{\rm det}$ corresponding to the minimum value of $P_{\rm out}$ is referred to as the sensing

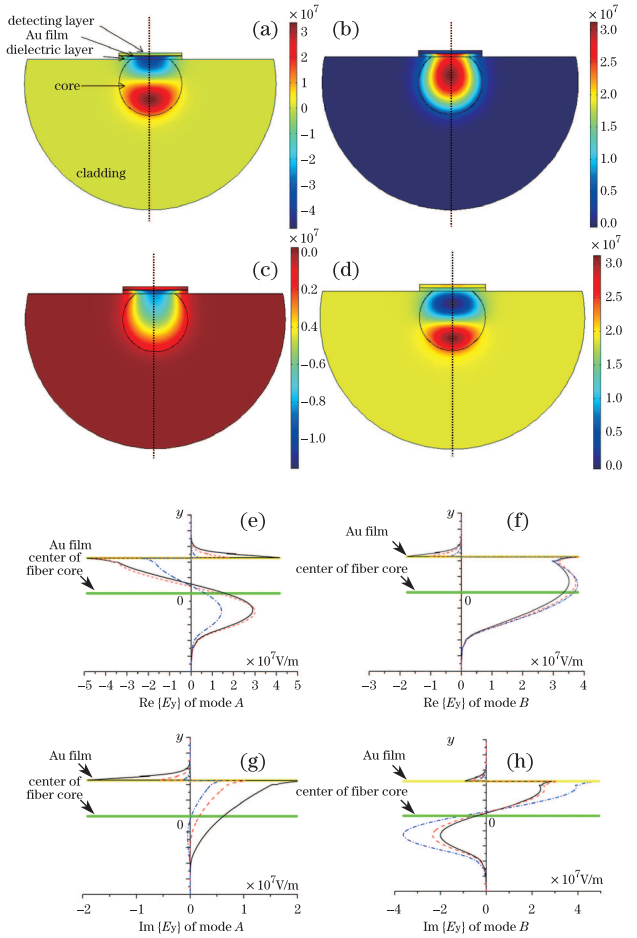

Fig. 3. (Color online) Field patterns of two eigenmodes, mode A and mode B, for $n_{\rm det} = 1.501$. Real part of modes (a) A and (b) B, respectively. Imaginary part of modes (c) A and (d) B, respectively. (e)-(h) Complex electric field profile of two eigenmodes for $h_{\rm det} = 500$ nm with $n_{\rm det} = 1.501$ (black solid line), $n_{\rm det} = 1.481$ (red dashed line), and $n_{\rm det} = 1.400$ (blue dotted chain line). (e) and (f) show the real part of modes A and B, respectively. (g) and (h) show the imaginary part of modes A and B, respectively.

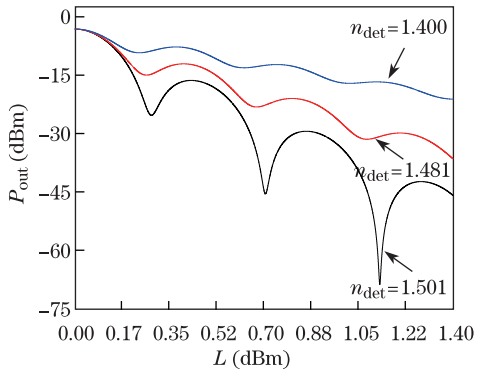

Fig. 4. Output power P_{out} (in dBm) as a function of the effective sensing length L with different refractive indices of the detecting layer, n_{det}.

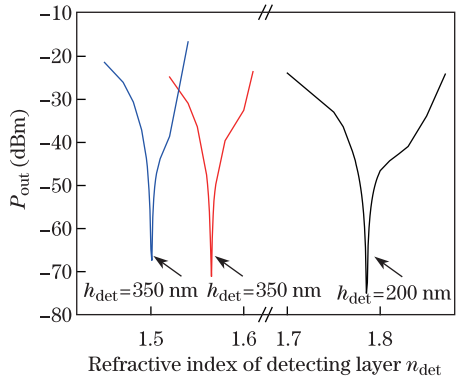

Fig. 5. Output power P_{out} (in dBm) as a function of the refractive index of detecting layer n_{det} under different detecting layer thicknesses, h_{det}.

center. Similarly, the sensing curve for detecting layers with thicknesses $h_{det} = 350$ nm and $h_{det} = 200$ nm can also be obtained (red and black solid lines, Fig. 5). Decreasing the thickness of detecting layer shifts the sensing center to a higher value because of the effective refractive index equality between SRSPP and optical fiber guided modes. The resolution of the sensor for 200 nm detecting layer, about one-eighth of wavelength, is evaluated according to the definition in Ref. [2]:

$$\text{Resolution} = \frac{f_{\text{Re}}}{\text{Sensitivity}} = f_{\text{Re}} \times \frac{\Delta n_{\text{det}}}{\Delta P_{\text{out}}}. \quad (1)$$

Around the sensing center $n_{det} = 1.785$, the average resolution is about 3.7×10^{-6} RIU in range of $\Delta n_{det} \sim 0.01$. The resolution of optical fiber SPP biosensor based on spectral interrogation is currently about 10^{-6} RIU for detecting the refractive index of a bulk substance[14,15]. The proposed sensor based on intensity interrogation can achieve a rather high resolution even for ultrathin layer detection.

For biochemical sensing, the reaction between an antibody and an antigen may be viewed as a model for tuning the thickness of an ultrathin detecting layer with fixed refractive index[16–18]. Therefore, the sensing characteristics of the sensor are studied according to the actual situation. As the refractive index of most biomolecules range from 1.4 to 1.7, the refractive index of the detecting layer n_{det} is fixed at 1.5. Figure 6 shows that P_{out} varies with h_{det} in the range of 450–550 nm, which indicates that a change of 5 nm in h_{det} around 500 nm corresponds to a change of about 30 dB in P_{out}. Similar to Ref. [10], the thickness-detection sensitivity (TDS) is defined as the variation of P_{out} over the corresponding change of h_{det}:

$$TDS = \Delta P_{\text{out}} / \Delta h_{\text{det}}. \quad (2)$$

Mean TDS is approximately 6.2 dB/nm, which is a high value for ultrathin layer detection. The ability of detecting thickness variation of tens of nanometers is crucial for biochemical sensing. Here, the antibody-antigen combination or a chemical reaction[19,20] always takes place on the metal surface with thickness of about tens of nanometers. Simulation results indicate that the proposed sensor is suitable for the small bio- or chemical molecule detection.

Aside from high sensitivity in ultrathin layer detection, the proposed optical fiber sensor also gives superiority in providing a flexible and adjustable sensitive region of the detecting layer thickness. Figure 7 shows that by fixing the refractive index of the detecting layer at $n_{det} = 1.5$ and varying the thickness of detecting layer h_{det} the sensing characteristics to h_{det} can be calculated under varying Au film thicknesses ($h_m = 32$, 34, and 36 nm). Notably, that when the thickness of the Au film h_m increases by 2 nm, the sensitive region of h_{det} shifts by approximately 67 nm because the Re$\{n_{eff}\}$ of SRSPP mode decreases with increased thickness of the Au film[21]. Therefore, a larger h_{det} is required to increase Re$\{n_{eff}\}$ of SRSPP and match with that of the fiber guided mode. In accordance with different surrounding media and sensing centers in the practical situation of biochemical sensing, the sensitive region of the detecting layer thickness can be adjusted by varying thickness of the Au film to satisfy the requirement.

In conclusion, an optical fiber sensor based on SRSPP mode is proposed, and the sensing characteristics are theoretically analyzed. This sensor could be applicable for ultrathin layer sensing. Even for the detecting layer with thickness about one-eighth of the wavelength, the resolution of this sensor could reach up to 3.7×10^{-6} RIU. This sensor is propitious for detection of small biochemical molecules, with a high thickness-detection sensitivity of 6.2 dB/nm. Moreover, the sensitive region of h_{det} is

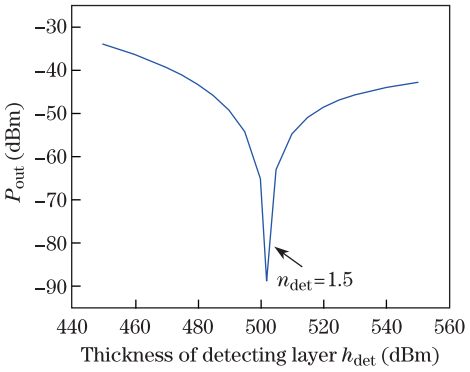

Fig. 6. Output power P_{out} (in dBm) as a function of the detecting layer thickness h_{det} with refractive index of detecting layer $n_{det} = 1.5$.

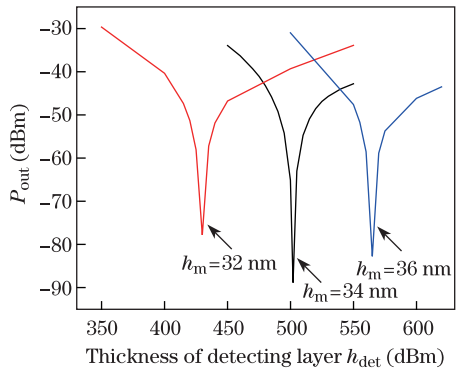

Fig. 7. Output power P_{out} (in dBm) as a function of the detecting layer thickness h_{det} labeled under different thicknesses of the Au film h_m.

can be easily extended by adjusting the structural parameters. All these properties allow the proposed sensor to be potentially useful as a compact and portable biochemical sensing system.

This work was supported by the National "973" Programs of China (Nos. 2013CBA01704, 2010CB327405, and 2011CBA00608) and the National Natural Science Foundation of China (Nos. 61036011, 61107050, and 61036010).

References

1. J. J. Burke, G. I. Stegeman, and T. Tamir, Phys. Rev. B **33,** 5186 (1986).
2. J. Homola, S. S. Yee, and G. Gauglitz, Sensor Actuator B Chem. **54,** 3 (1999).
3. J. Homola, Anal. Bioanal. Chem. **377,** 528 (2003).
4. X. D. Hoa, A. G. Kirk, and M. Tabrizian, Biosens. Bioelectron. **23,** 151 (2007).
5. R. D. Roy, R. Chattopadhyay, and S. K. Bhadra, Photon. Res. **1,** 164 (2013).
6. Y. Wu and Z. Gu, Chin. Opt. Lett. **10,** 081301 (2012).
7. R. Wan, F. Liu, and Y. Huang, Opt. Lett. **35,** 244 (2010).
8. J. Guo, P. D. Keathley, and J. T. Hastings, Opt. Lett. **33,** 512 (2008).
9. B. Fan, F. Liu, Y. Li, Y. Huang, Y. Miura, and D. Ohnishi, Appl. Phys. Lett. **100,** 111108 (2012).
10. B. Fan, F. Liu, X. Wang, Y. Li, K. Cui, and Y. Huang, Appl. Phys. Lett. **102,** 061109 (2013).
11. E. D. Palik, *Handbook of Optical Constants of Solids* (Academic, Waltham, 1985).
12. COMSOL AB, *FEMLAB RF Module Model Library* (3.3 edition, Sweden, 2006).
13. W. Huang, J. Opt. Soc. Am. A **11**, 963 (1994).
14. H. S. Jang, K. N. Park, C. D. Kang, J. P. Kim , S. J. Sim, and K. S. Lee, Opt. Commun. **282,** 2827 (2009).
15. R. Slavik, J. Homola, J. Ctyroky, and E. Brynda, Sensor Actuator B Chem. **74,** 106 (2001).
16. M. Malmqvist, Curr. Opin. Immunol. **5,** 282 (1993).
17. R. Karlsson, A. Michaelsson, and L. Mattsson, J. Immunol. Meth. **145,** 229 (1991).
18. L. G. Fagerstam, A. Frostell, R. Karlsson, M. Kullman, A. Larsson, M. Malmqvist, and H. Butt, J. Mol. Recogn. **3,** 208 (1990).
19. O. Salihoglu, S. Balci, and C. Kocabas, Appl. Phys. Lett. **100,** 213110 (2012).
20. K. Hegnerova and J. Homola, Sensor Actuator B Chem. **151,** 177 (2010).
21. Z. Han, S. I. Bozhevolnyi, Rep. Progr. Phys. **76,** 16402 (2013).